RMetS
Royal Meteorological Society

Observational evidence for the mechanism of the poleward propagation of zonal wind anomalies over the North Atlantic

Jiacan Yuan[a]*, Sukyoung Lee[b] and Benkui Tan[a]

[a]*Department of Atmospheric and Oceanic Sciences, School of Physics, Peking University, Beijing, China*
[b]*Department of Meteorology, Pennsylvania State University, State College, PA, USA*

*Correspondence to: J. Yuan, Department of Atmospheric and Oceanic Sciences, School of Physics, Peking University, Beijing 100871, China. E-mail: jiacan.yuan@gmail.com

This study examines the physical mechanisms that drive the poleward propagation of zonal-mean flow anomalies over the North Atlantic during the boreal winter with ECMWF ERA40 reanalysis data that spans the years 1958–2001. An empirical orthogonal function (EOF) analysis is performed on the zonal wind anomalies for the North Atlantic domain. Based on time-lag correlations between the first two EOFs, 14 poleward propagation events are identified.

A series of lagged composite calculations of the poleward propagation events reveals the following processes: midlatitude synoptic-scale Rossby waves propagate equatorward and break when they encounter their critical latitudes in the Tropics and Subtropics; a new critical latitude is generated slightly poleward of the previous critical latitude, and the subsequent wave breaking occurs at this new critical latitude. This interaction between the wave breaking and the critical latitude drives the poleward propagation of zonal-mean zonal wind anomaly. A comparison between the poleward propagation events and zonal index events indicates that the poleward propagation is associated with a relatively weak potential vorticity gradient over the Subtropics. These North Atlantic poleward propagation events are found to be preceded by anomalously strong transient eddy activity over the subtropical North Pacific, and by anomalously weak tropical convection over the tropical Atlantic Ocean and the Amazon. **Copyright © 2012 Royal Meteorological Society**

Key Words: poleward propagation; wave breaking; critical latitude; North Atlantic

Received 7 December 2011; Revised 26 June 2012; Accepted 3 July 2012; Published online in Wiley Online Library 17 September 2012

Citation: Yuan J, Lee S, Tan B. 2013. Observational evidence for the mechanism of the poleward propagation of zonal wind anomalies over the North Atlantic. *Q. J. R. Meteorol. Soc.* **139**: 992–998. DOI:10.1002/qj.2010

1. Introduction

Zonally averaged flow variability has been of great research interest in recent decades because it is closely associated with variations in both transient and stationary waves, which influence the weather and climate. The poleward propagation of tropospheric zonal-mean flow anomalies (hereafter simply referred to as 'poleward propagation') is one form of zonal-mean flow variability. Evidence of this poleward propagation was first shown in the observational study of Riehl *et al.* (1950). James *et al.* (1994) found that similar poleward propagation can also occur in an idealized model. These findings were followed by studies that investigated the mechanisms driving the poleward propagation.

With a barotropic weakly nonlinear model, James and Dodd (1996) suggested that the poleward propagation originated from the interaction between the mean flow and equatorward-propagating Rossby waves from middle and high latitudes. Specifically, an eddy momentum flux convergence occurs at the poleward flank of a positive zonal wind anomaly and thus causes the positive zonal wind anomaly to shift poleward. According to the study of Robinson (2000), a poleward shift in low-level baroclinicity

may play an important role in driving the poleward propagation. The observations of Feldstein (1998) show that the transient eddy momentum flux convergence contributes to the poleward propagation, and this finding is consistent with both of the above mechanisms.

In the modelling study of Lee *et al.* (2007, hereafter L07), it was shown that the poleward propagation is initiated in the Tropics by the breaking of Rossby waves which are generated in midlatitudes. This wave breaking deposits negative zonal momentum, decelerating the ambient zonal wind. This results in a poleward shift in the location of the critical latitude (where the phase speed of the wave is equal to the ambient zonal-mean zonal wind speed), and a reduction in the meridional potential vorticity gradient. As a result, subsequent midlatitude waves break poleward of the previous critical latitude. In this manner the zonal-mean flow anomalies propagate poleward, together with the critical latitude and the region with the small meridional potential vorticity gradient. Building upon this finding, the primary aim of this study is to further examine whether the dynamical processes described in L07 operate in the atmosphere. In this study, we will focus on the poleward-propagating zonal wind anomalies over the North Atlantic. Here we apply the theories of eddy-zonal mean flow interaction for the North Atlantic sector. Although this is not a precise application of the theory, we justify its use based on the finding that the zonal convergence of the sector-mean eddy momentum flux is much smaller than the meridional convergence of the sector-mean eddy momentum flux (not shown).

There is evidence that tropical forcing can modify the circulation over the North Atlantic (e.g. Nigam *et al.*, 1986, 1988; Hoskins *et al.*, 1987). At the interdecadal time-scale, Rajagopalan *et al.* (1998) found that tropical Atlantic sea surface temperature (SST) anomalies significantly influence North Atlantic climate variability. At the intraseasonal time-scale, Feldstein (1999) showed that the angular momentum flux undergoes poleward propagation in association with the Madden–Julian Oscillation (Madden and Julian, 1971, 1972). The diagnostic study of Yuan *et al.* (2011) suggests that convection over the tropical Indian and western Pacific Oceans excites fluctuations of the North Atlantic jets, through the circumglobal teleconnection wave packet (Branstator, 2002; Feldstein and Dayan, 2008). Motivated by these findings, another aim of our study is to investigate whether tropical convection has an influence on the poleward propagation in the North Atlantic region.

The data and methodology are described in section 2. Section 3 presents the diagnostic results. The conclusion and discussion are given in section 4.

2. Data and methodology

This study uses the daily European Centre for Medium-Range Weather Forecasts (ECMWF) ERA-40 reanalysis data (Uppala *et al.*, 2005) for the months of November, December, January, February and March. The time period is from 1958 to 2001. To obtain the main characteristics of the North Atlantic jet, we perform three-dimensional empirical orthogonal function (EOF) analysis on the zonal wind in the same manner as Yuan *et al.* (2011). The analysis domain spans 50°W–20°E, 10°N–80°N, over seven vertical levels: 100, 150, 200, 250, 300, 400, 500 hPa. The time series of the first and the second loadings are referred to as PC1 and PC2, respectively. Given the first and second EOF loading patterns (Figure 1), it can be inferred that the poleward propagation would occur if PC2 leads PC1; because the observed period of the poleward propagation is about 40–60 days (Feldstein, 1998), PC2 is expected to lead PC1 by about 10–15 days. Accordingly, we select the poleward propagation events as follows: firstly, the years in which PC2 leads PC1 by less than 20 days are identified; next, we select those years when the maximum lag correlation is greater than 0.4. There are 14 years that satisfy these criteria: 1960, 1966, 1967, 1969, 1970, 1971, 1980, 1981, 1983, 1985, 1986, 1988, 1990 and 1996. For each of these 14 poleward propagation years, we compute the 250 hPa $[u]'$, where u denotes zonal wind, the square brackets a longitudinal sector mean between 50°W and 20°E, and the prime the deviation from the time mean of 44 winters. Since the poleward propagation is most clearly visible between the Equator and 50°N latitude (see Figure 2a in Lee *et al.*, 2007), we choose $[u]'$ at 25°N as an index for our composite analysis. For each year, within the 3-month period of December, January and February, the day when this index reaches its minimum is regarded as the lag-0 day. The minimum $[u]'$ is chosen based on the hypothesis that zonal mean flow deceleration by wave breaking drives the poleward propagation. A poleward propagation event is defined as extending from 15 days before to 15 days after the lag-0 day. This procedure produced 14 events.

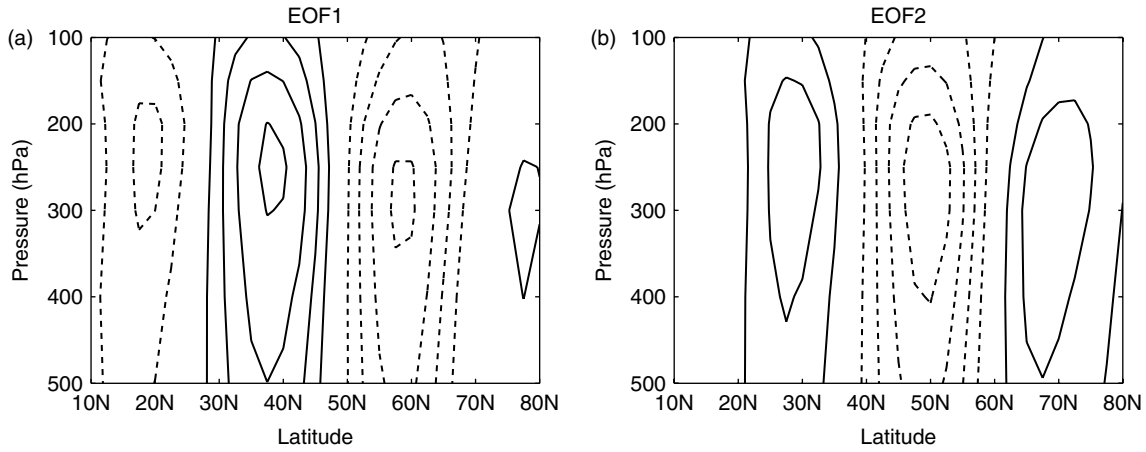

Figure 1. Spatial structure of the North Atlantic jet loading patterns for (a) EOF1 (18.6%) and (b) EOF2 (16.5%) at 30°W. Solid lines denote positive values, and dashed lines negative values. The contour interval is 0.01, and the zero contour has been omitted.

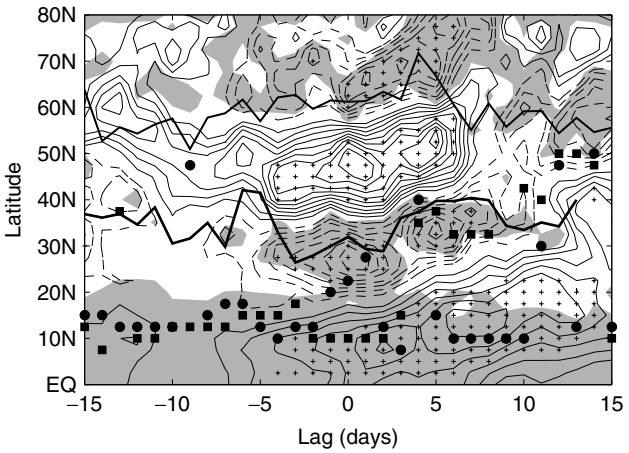

Figure 2. Composite anomalous zonal wind (contours) and critical latitudes (markers), on the 250 hPa surface. The solid contours denote a positive wind anomaly and the dashed contours denote a negative wind anomaly. The zero contour is omitted and contour interval is 1 m s^{-1}. The circle and square markers represent the critical latitudes corresponding to the low- and mid-latitude sets, respectively. The shading indicates regions where $|\partial[q]/\partial y|$ is less than 5×10^{-11} m^{-1} s^{-1}. The heavy thick solid line represents the LC index for PV range from 0.5 to 3 PVU at 330 K isentropic surface, and the medium thick solid line the LC index for PV range from 1 to 3.5 PVU at 310 K isentropic surface (see text for detail). The pluses mark the area where values of $[u]'$ are statistically significant above the 95% confidence level.

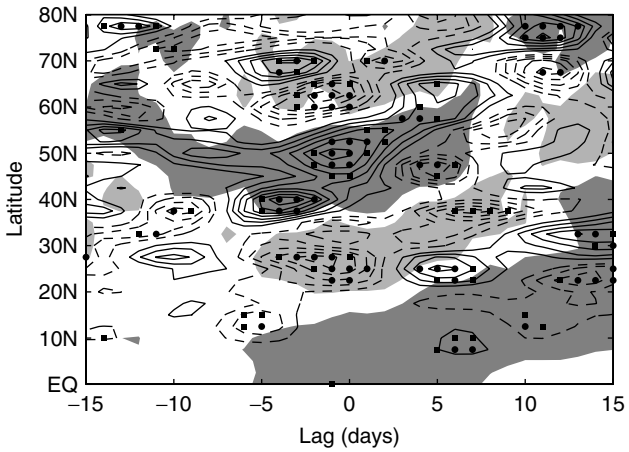

Figure 3. Hovmöller diagram of the composite $-\partial[u^*v^*]'/\partial y$ based on the poleward-propagating events, on the 250 hPa surface. The dashed lines denote negative values, while the solid lines denote positive values. The zero contour is omitted. Contour interval is 1×10^{-5} m s^{-2}. The shadings are for the composite 250 hPa $[u]'$ as in Figure 2. The dark (light) shading is for values greater (less) than 2 m s^{-1} (-2 m s^{-1}). The circle and square markers represent the area where values of $-\partial[u^*v^*]'/\partial y$ are statistically significant above the 95% and 90% confidence levels, respectively.

For the composites of zonally varying fields, we perform a zonal shift to prevent the cancellation in wave phase between different events. To carry out this calculation, we first define the reference longitude as the longitudinal grid point at which u' at 25°N on lag-0 day is a minimum. The longitudinal interval examined is from 50°W to 20°E. For each event, the reference longitude is fixed for all lag days, and the field in question is shifted in such a manner that the reference longitude is located at the centre of the longitudinal range. The composite was obtained by averaging these phase-shifted fields. The reference longitude of the 14 events ranges from 45°W to 15°E.

The critical latitudes are identified by first calculating the phase speed using the expression $ma\cos\varphi$, where m is an estimated angular velocity of the Rossby wave, a is the radius of the Earth and φ is the latitude. To estimate m, we calculated one-point lag correlations of meridional wind over the North Atlantic region (75°W–45°E), for each latitude from 0° to 90°N (not shown). Then m is obtained by $\delta\lambda/\delta t$, where $\delta\lambda$ is the longitudes that the Rossby wave has passed during δt days. This calculation revealed that there are two latitudinal intervals with distinctive m values: between 25°N and 37.5°N, the average value of m is 1.82×10^{-6} rad s^{-1}; between 40°N and 50°N, the average value of m is 2.29×10^{-6} rad s^{-1}. Using these values, we obtained two sets of phase speeds which are functions of latitude. The set calculated with $m = 1.82 \times 10^{-6}$ rad s^{-1} will be referred to as the 'low-latitude' set, while the other set will be referred to as the 'mid-latitude' set. For each set, $|[u] - c|$ is calculated at all latitudinal grid points between the Equator and 50°N, and the latitude at which $|[u] - c| \leq 1$ is identified as a critical latitude. Here $[u]$ denotes the zonally averaged zonal wind over the 75°W–45°E sector.

To evaluate the statistical significance of non-Gaussian fields (meridional gradient of quasi-geostrophic potential vorticity, convective precipitation and meridional wind variance), we used a Monte Carlo approach. For this purpose, 1000 composites are generated, with each composite consisting of 14 randomly selected days from the 1958–2001 period. Statistically significant levels are evaluated based on the distribution of the 1000 random samples at each grid point. The statistical significance of the zonal wind anomaly composite is obtained with Student's t-test.

3. Results

3.1. Evolution of poleward propagation

We first examine whether the composite $[u]'$ exhibits the anticipated poleward propagation. This composite, indicated by the contours in Figure 2, indeed shows that statistically significant $[u]'$ undergoes poleward propagation, although it is confined mostly to between lag -5 days and lag +14 days. This appearance of the poleward propagation indicates that our criteria can indeed identify poleward-propagating events. Between lag -5 days and lag +14 days, Figure 2 shows that the critical latitudes also exhibit poleward propagation. There is a hint that this poleward propagation is accompanied by a band with weak meridional gradients in the quasi-geostrophic potential vorticity ($\partial[q]/\partial y$, where the zonal average is taken from 75°W to 45°E). Because wave breaking tends to coincide with its critical latitude (Killworth and McIntyre, 1985), this relationship suggests that wave breaking plays a central role in generating the negative $[u]'$ anomaly and its poleward propagation. In addition, the weakened $\partial[q]/\partial y$, by reducing the refractive index (Palmer, 1982), can act as a barrier to the subsequent equatorward wave propagation. This may help to explain why wave breaking does not occur equatorward of the latitudes where $\partial[q]/\partial y$ is relatively weak.

We also examine the anomalous eddy momentum flux convergence at 250 hPa (Figure 3). The momentum flux convergence is smoothed with a 7-day low-pass filter before the composite calculation. As a reference, the $[u]'$ composite is indicated with shading. Figure 3 shows that the anomalous eddy momentum flux convergence

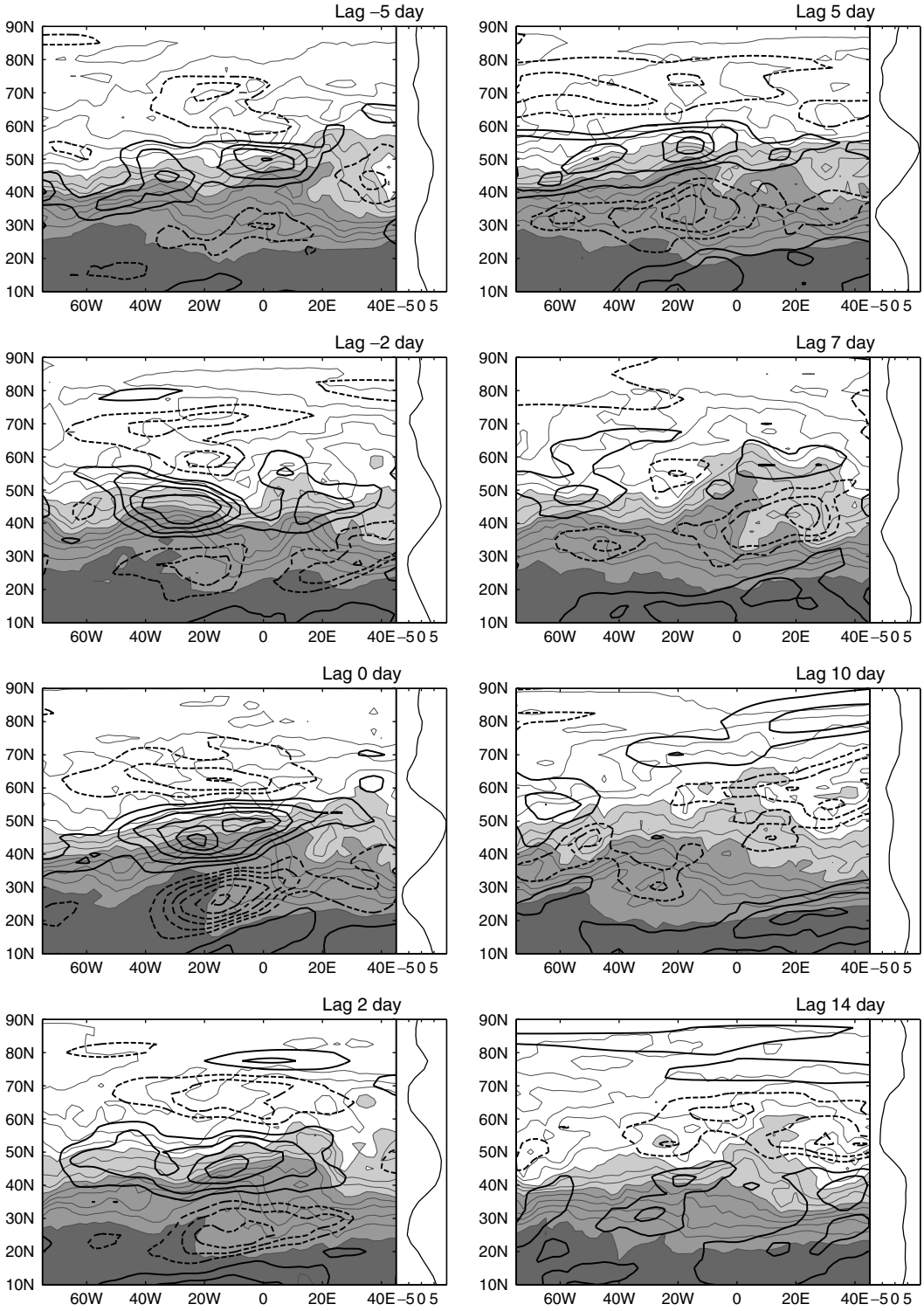

Figure 4. Lagged composite potential vorticity (thin contours) on the $\theta = 330$ K isentropic surface based on the poleward propagation events. The abscissa denotes the longitude and the ordinate indicates the latitude. The contour interval is 0.5 PVU (1 potential vorticity unit (PVU) $=10^{-6}$ m^2 s^{-1} K kg^{-1}). The PV value marking the boundary between the dark and the grey shading is 0.5 PVU. Similarly, the PV values marking the boundary between the grey shading and light shading is 3 PVU, and between light shading and no shading 4.5 PVU. The black thick contours denote the composite of the zonal wind anomaly at each lag day. The interval is 4 m s^{-1}. Solid (dashed) lines are for positive (negative) values, and zero lines are omitted. The right margin of each panel shows the zonal mean of the composite zonal wind anomaly.

$-\partial[v^*u^*]'/\partial y$ propagates poleward, slightly leading $[u]'$. This is consistent with the modelling results of Lee *et al.* (2007), and suggests that $[u]'$ is driven by the anomalous eddy momentum flux convergence.

We performed a PV-θ analysis (Hoskins *et al.*, 1985) to diagnose the wave-breaking feature. Ertel's potential vorticity (PV) contours on the $\theta = 330$ K isentropic surface is analysed because the the 330 K surface in the Subtropics is located at the upper troposphere. The time evolution of the PV and u' fields indicates that the negative $[u]'$ band is indeed associated with wave breaking (Figure 4). As a reference, the zonal average of u' is also shown in the right

margin of each panel. As was suggested by L07, we focus on the negative $[u]'$ because this particular anomaly coincides with wave breaking. Between lag −5 days and lag −2 days, a negative $[u]'$ band is weak and vacillating near 30°N. This is associated with wave overturning, as is revealed by the 0.5-PVU contour. By the lag-0 day, the signature of wave overturning is clearer and the negative $[u]'$ band becomes more pronounced. During the wave breaking, the centre of the negative $[u]'$ band shifts poleward, from 30°N to 35°N (between lag-0 day and lag +5 days in Figure 4). It is important to note that a positive $[u]'$ band forms at both northern and southern edges of the negative $[u]'$. This positive–negative–positive tripole structure of $[u]'$ is associated with the intensified PV gradients at both sides of the wave-breaking region.

This first wave-breaking episode is followed by another wave overturning at higher latitude. By lag +7 days, the centre of the negative $[u]'$ band rapidly shifts to 38°N, and the 3-PVU contour overturns dramatically in the neighbourhood. At lag +10 days, the 3-PVU contour becomes mild. Instead, the 4.5-PVU contour overturns, resulting in formation of the negative $[u]'$ band centred at 60°N. By lag 14 days, the 4.5-PVU contour steepens, and the high-latitude negative $[u]'$ band intensifies.

In order to objectively identify the location of wave breaking, we calculate the wave-breaking index of Akahori and Yoden (1997). Following these authors, we refer to this index as the LC index. For each longitudinal grid point from 75°W to 45°E on an isentropic surface, we first identify a latitudinal band bounded by two particular PV contours. Next, we compute the meridional gradient of PV within this band, and then identify the location of wave breaking by the latitude where the PV gradient is negative. More precisely, the LC index is obtained by calculating

$$\mathrm{LC} = \frac{1}{S}\sum_{i=1}^{n} \varphi_i \times \left(\frac{\partial \mathrm{PV}}{\partial y}\right)_i, \tag{1}$$

$$S = \sum_{i=1}^{n} (\partial \mathrm{PV}/\partial y)_i, \tag{2}$$

where n is the number of grid points at which the PV gradient is negative, and φ the latitude. In other words, the LC index is a measure of the latitude of wave breaking. To diagnose the subtropical wave breaking, we chose the PV range to be 0.5–3.0 PVU on the 330 K surface. As can be seen from Figure 2, between lag −3 and +5 days this LC index (heavy thick line) propagates poleward from 26°N to about 40°N. While this LC index is not exactly co-located with the local $[u]'$ minimum, and instead is located a few degrees poleward, the LC index does propagate poleward in tandem with the subtropical band of negative $[u]'$. For later positive lags, the negative $[u]'$ band moves into the Extratropics (Figure 2). Since isentropes tilt upward with latitude, the 330 K surface is not suitable for diagnosing extratropical wave breaking; hence instead we examine the 310 K surface. For this extratropical LC index, the PV range chosen is 1.0–3.5 PVU. Similar to the subtropical LC index, this extratropical LC index (medium thick line in Figure 2) also displays some poleward propagation, consistent with the negative $[u]'$ anomaly propagation at mid and high latitudes. From this relationship between the LC index and the negative $[u]'$ bands, we conclude that the poleward propagation of the negative $[u]'$ is driven by a series wave breaking.

3.2. *Meridional potential vorticity gradient, tropical heating and upstream transient eddies*

In their modelling study, Son and Lee (2006) showed that zonal mean flow variability corresponds to either the zonal index (ZI) or to poleward zonal mean anomaly propagation. They found that $\partial[q]/\partial y$ is relatively weak in the poleward propagation regime and strong in the ZI regime. Because meridional wave propagation is hindered when $\partial[q]/\partial y$ is sharp and strong (Swanson *et al.*, 1997), the above relationship suggests that at least in their model the poleward propagation of $[u]'$ is driven by equatorward propagating waves. Therefore, using the ZI events defined in Yuan *et al.* (2011), we examine whether these relationships also hold in the observations. (The ZI events describe the north–south meander of the North Atlantic jet. During positive events, the eddy-driven jet is centred near 60°N and the subtropical jet near 20°N. During negative events, the eddy-driven jet and the subtropical jet merge together and form a single jet located at 40°N. There are 42 positive and 42 negative ZI events.) Figure 5 shows the composite $\partial[q]/\partial y$ for the poleward-propagating events minus the composite $\partial[q]/\partial y$ for the ZI events. Between lag −5 and lag +1 days, there is a band of negative anomalous $\partial[q]/\partial y$ near 30°N, indicating that during the onset of the poleward propagation the subtropical $\partial[q]/\partial y$ is significantly weaker for the poleward-propagating events than for the ZI events. The weak $\partial[q]/\partial y$ band persists between lag +2 and lag +10 days, but the location shifts poleward and the amplitude declines. This is consistent with the conclusion by Son and Lee (2006) that a relatively weak $\partial[q]/\partial y$ provides a favourable condition for the poleward-propagating events.

Son and Lee (2006) also found in their model that the strength of the subtropical $\partial[q]/\partial y$ was controlled by the imposed tropical heating; weak tropical heating generates weak subtropical $\partial[q]/\partial y$. Therefore, we examine convective

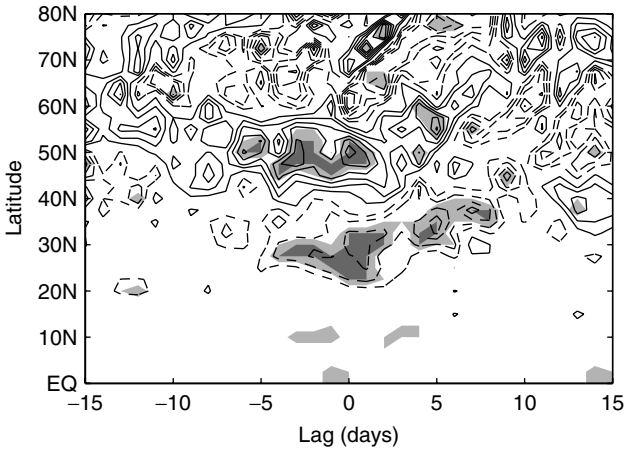

Figure 5. Hovmöller diagram of the composite $\partial[q]/\partial y$ for the poleward-propagating events minus the composite $\partial[q]/\partial y$ for the ZI events, on the 250 hPa surface. The dashed lines denote negative values, while the solid lines denote positive values. The zero contour is omitted. Contour interval is 1×10^{-11} m^{-1} s^{-1}. The dark and light shading indicates those regions in which the difference between the poleward propagation event composites and the ZI event composites are statistically significant above the 95% and 90% confidence levels, respectively.

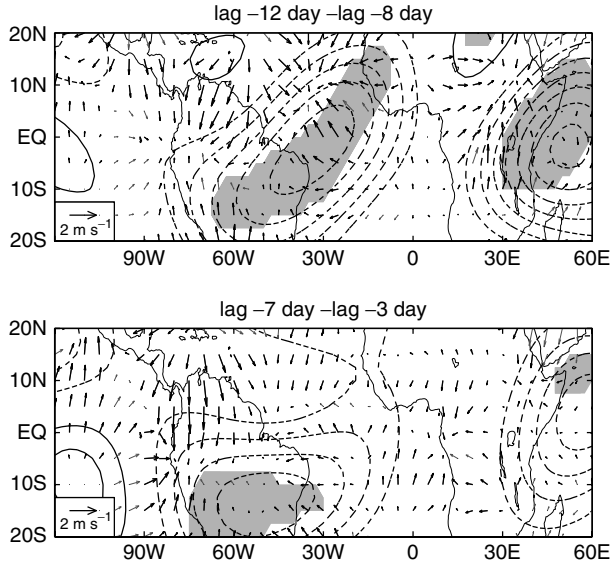

Figure 6. Lagged composite of anomalous convective precipitation based on the poleward propagation events. The title of every panel reveals the 5 days of the pentad average. The solid lines denote positive values and the dashed lines denote negative values. The zero line is omitted. The contour interval is 1×10^{-4} m. Shaded areas indicate values that are statistically significant above the 95% confidence level. The arrows indicate the anomalous divergent wind at 250 hPa. Heavy arrows indicate divergent wind anomalies that are statistically significant above the 95% confidence level.

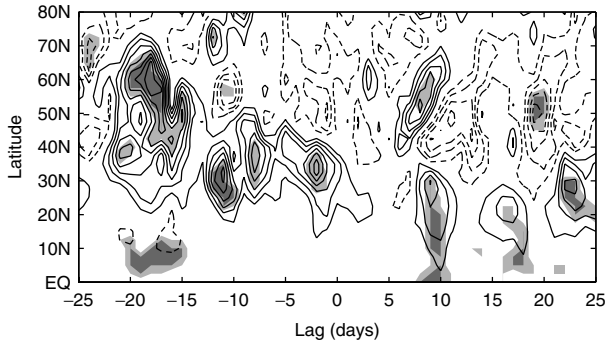

Figure 7. Hovmöller diagrams of the 250 hPa anomalous eddy variance based on poleward propagation events. The results are zonally averaged over 180–50°W. The abscissa denotes the time-lag and the ordinate indicates the latitude. Solid lines indicate positive values and dashed lines negative values. The zero line is omitted. The interval is 20 $m^2 s^{-2}$. The dark and light Shaded areas indicate values that are statistically significant above the 95% and 90% confidence level, respectively.

precipitation data as a proxy of the tropical convective heating, to investigate whether the tropical convective heating is anomalously weak prior to the initial excitation of the poleward propagation. Figure 6 shows pentad-average lagged composites of convective precipitation and 250 hPa divergent wind anomalies, again based on the poleward propagation events. Between lag −12 and lag −8 days (Figure 6(a)), statistically significant negative anomalies in convective precipitation appear over the tropical Atlantic Ocean and the Amazon. (A field significance test (Livezey and Chen, 1983; Feldstein and Franzke, 2006) indicates that the area encompassed by these anomalies is statistically significant at the 95% confidence level.) Consistent with this result, in the region surrounding the negative precipitation anomaly centre there is a negative divergent wind anomaly in the upper troposphere. These features also persist between lag −7 and lag −3 days (Figure 6(b)), but they do not pass the field significance test. Together with the anomalously weak $\partial[q]/\partial y$, these results suggest that anomalously weak tropical convection provides favourable conditions for tropical wave breaking which can initiate a poleward propagation episode.

L07 found that prior to the lag-0 day the eddy kinetic energy (EKE) is anomalously large, and after the lag-0 day the EKE becomes anomalously weak. If similar behaviour in the EKE is associated with the North Atlantic poleward propagation, it may be that the poleward propagation is preceded by anomalously strong EKE upstream of the North Atlantic region. To investigate this possibility, we examined the 250 hPa eddy meridional wind variance anomaly, averaged between 180° and 50°W (see Figure 7). In the Subtropics, anomalously large eddy variance can indeed be seen prior to the lag-0 day. Afterwards, the eddy variance becomes anomalously small. This suggests that poleward propagation in the North Atlantic sector is preceded by anomalously intense transient eddy activity over the subtropical North Pacific Ocean. The field significance test is also performed here, and the result shows that the area enclosed by the anomalies is significant at the 95% confidence level.

4. Discussion and conclusions

In this study, we investigated the dynamic mechanisms that drive the observed poleward-propagating zonal wind anomalies over the North Atlantic during the boreal winter. Our analysis shows that this poleward propagation is driven by a series of Rossby wave-breaking events which occur when equatorward propagating Rossby waves encounter their critical latitudes. The wave breaking generates a new critical latitude slightly poleward of the previous critical latitude, and these mutual interactions between the critical latitude and wave breaking drive the poleward propagation. This result is consistent with the findings of L07.

As suggested in the modelling study of Son and Lee (2006), the existence of poleward propagation is found to be associated with a relatively weak quasi-geostrophic potential vorticity gradient for the background flow. We compared $\partial[q]/\partial y$ of the poleward propagation events with that of the zonal index events. The results (Figure 5) indicate that $\partial[q]/\partial y$ during the poleward propagation is weaker than that during the ZI events in the subtropical region. There is also evidence that the North Atlantic poleward propagation events are preceded by anomalously weak tropical convection over the tropical Atlantic Ocean and Amazon basin, as well as by anomalously strong transient eddy activity over the North Pacific. These conditions, respectively, are again consistent with the modelling studies of Son and Lee (2006) and L07, supporting the conclusions of L07 that a relatively weak meridional potential vorticity gradient in the Subtropics, generated by relatively weak tropical heating, is conducive to tropical wave breaking which can then initiate a poleward propagation event. However, in nature, where the strength of the tropical heating is not 'imposed' in the same sense as in the model, the findings in this study raise the following questions. How might the convection over the tropical Atlantic and the Amazon be linked to the Pacific transient eddy activity? Are they independent of each other? Or is there a process that orchestrates both of these processes, and if so how will this process change as the climate continues to warm? It would

be worth addressing these questions with the ever-increasing volume of reanalysis datasets and climate models, as well as with idealized models.

Acknowledgements

This research is supported by the Chinese NSF (grants 40875027, 41130962), the Chinese Scholarship Council, the PhD Programs Foundation of the Ministry of Education of China (grant 200800010026) and by National Science Foundation (grants AGS-1036858 and AGS-1139970). We thank Dr Feldstein for offering beneficial suggestions and comments. We would like to thank the European Centre for Medium-Range Weather Forecasts (ECMWF) for providing us with the ERA-40 reanalysis data. We would also like to thank two anonymous reviewers for their helpful comments.

References

Akahori K, Yoden S. 1997. Zonal flow vacillation and bimodality of baroclinic eddy life cycles in a simple global circulation model. *J. Atmos. Sci.* **54**: 2349–2361.

Branstator G. 2002. Circumglobal teleconnections, the jet stream waveguide, and the North Atlantic Oscillation. *J. Climate* **15**: 1893–1910.

Feldstein SB. 1998. An observational study of the intraseasonal poleward propagation of zonal mean flow anomalies. *J. Atmos. Sci.* **55**: 2516–2529.

Feldstein SB. 1999. The atmospheric dynamics of intraseasonal length-of-day fluctuations during the austral winter. *J. Atmos. Sci.* **56**: 3043–3058.

Feldstein SB, Dayan U. 2008. Circumglobal teleconnections and wave packets associated with Israeli winter precipitation. *Q. J. R. Meteorol. Soc.* **134**: 455–467.

Feldstein SB, Franzke C. 2006. Are the North Atlantic Oscillation and the Northern Annular Mode distinguishable? *J. Atmos. Sci.* **62**: 2915–2930.

Hoskins BJ, McIntyre EM, Robertson WA. 1985. One the use and significance of isentropic potential vorticity maps. *Q. J. R. Meteorol. Soc.* **111**: 977–946.

Hoskins BJ, Sardeshmukh PD. 1987. A diagnostic study of the dynamics of northern hemisphere winter of 1985–86. *Q. J. R. Meteorol. Soc.* **113**: 759–778.

James IN, Dodd JP. 1996. A mechanism for the low frequency variability of the midlatitude troposphere. *Q. J. R. Meteorol. Soc.* **122**: 1197–1210.

James PM, Fraedrich K, James IN. 1994. Wave-zonal flow interaction and ultra-low-frequency variability in a simplified global general circulation model. *Q. J. R. Meteorol. Soc.* **120**: 1045–1067.

Killworth PD, McIntyre ME. 1985. Do Rossby-wave critical layers absorb, reflect or over-reflect? *J. Fluid Mech.* **161**: 449–492.

Lee S, Son S, Grise K, Feldstein SB. 2007. A mechanism for the poleward propagation of zonal mean flow anomalies. *J. Atmos. Sci.* **64**: 849–868.

Livezey RE, Chen WY. 1983. Statistical field significance and its determination by Monte Carlo techniques. *Mon. Weather Rev.* **111**: 46–59.

Madden R, Julian P. 1971. Detection of a 40–50 day oscillation in the zonal wind in the tropical Pacific. *J. Atmos. Sci.* **28**: 702–708.

Madden R, Julian P. 1972. Description of global-scale circulation cells in the tropics with a 40–50 day period. *J. Atmos. Sci.* **29**: 1109–1123.

Nigam S, Held IM, Lyons SW. 1986. Linear simulation of the stationary eddies in a general circulation model. Part I: The no-mountain model. *J. Atmos. Sci.* **43**: 2944–2961.

Nigam S, Held IM, Lyons SW. 1988. Linear simulation of the stationary eddies in a general circulation model. Part II: The 'mountain' model. *J. Atmos. Sci.* **45**: 1434–1452.

Palmer TN. 1982. Properties of the Eliassen–Palm flux for planetary scale motions. *J. Atmos. Sci.* **39**: 992–997.

Rajagopalan B, Kushnir Y, Tourre YM. 1998. Observed decadal midlatitude and tropical Atlantic climate variability. *Geophys. Res. Lett.* **25**: 3967–3970.

Riehl T, Yeh C, LaSeur NE. 1950. A study of variations of the general circulation. *J. Meteorol.* **7**: 181.

Robinson W. 2000. Baroclinic mechanism for the eddy feedback on the zonal index. *J. Atmos. Sci.* **57**: 415–422.

Son S, Lee S. 2006. Preferred modes of variability and their relationship with climate change. *J. Climate* **19**: 2063–2075.

Swanson KL, Kushner PJ, Held IM. 1997. Dynamics of barotropic storm tracks. *J. Atmos. Sci.* **54**: 791–810.

Uppala SM, Kållberg PW, Simmons AJ, Andrae U, Da Costa Bechtold V, Fiorino M, Gibson JK, Haseler J, Hernandez A, Kelly GA, Li X, Onogi K, Saarinen S, Sokka N, Allan RP, Andersson E, Arpe K, Balmaseda MA, Beljaars ACM, Van De Berg L, Bidlot J, Bormann N, Caires S, Chevallier F, Dethof A, Dragosavac M, Fisher M, Fuentes M, Hagemann S, Hólm E, Hoskins BJ, Isaksen L, Janssen PAEM, Jenne R, Mcnally AP, Mahfouf J-F, Morcrette J-J, Rayner NA, Saunders RW, Simon P, Ster A, Trenberth KE, Untch A, Vasiljevic D, Viterbo P, Woollen J. 2005. The ERA-40 reanalysis. *Q. J. R. Meteorol. Soc.* **131**: 2961–3012.

Yuan J, Feldstein SB, Lee S, Tan B. 2011. The relationship between the North Atlantic jet and tropical convection over the Indian and western Pacific Oceans. *J. Climate* **24**: 6100–6113.

